Smart Structures and Systems, *Vol. 27, No. 3 (2021) 507-523*
DOI: https://doi.org/10.12989/sss.2021.27.3.507

Crack prediction in pipeline using ANN-PSO based on numerical and experimental modal analysis

Meriem Seguini [1a], Samir Khatir*[2], Djilali Boutchicha [3b], Djamel Nedjar [1c] and Magd Abdel Wahab [4,5d]

[1] *Laboratory of Mechanic of Structures and Stability of Constructions LM2SC, Faculty of Architecture and Civil Engineering, Laboratory of Applied Mechanics, University of Sciences and Technology of Oran Mohamed Boudiaf, Bp 1505 Elmenouar Oran, Algeria*
[2] *Faculty of Civil Engineering, Ho Chi Minh City Open University, Ho Chi Minh City, Viet Nam*
[3] *LMA, Mechanical Engineering Department, USTO-MB, BP 1055 El Menaour, Oran 31000, Algeria*
[4] *Institute of Research and Development, Duy Tan University, 03 Quang Trung, Da Nang 550000, Viet Nam*
[5] *Soete Laboratory, Faculty of Engineering and Architecture, Ghent University, Technologiepark Zwijnaarde 903, B-9052, Zwijnaarde, Belgium*

(*Received January 31, 2020, Revised January 13, 2021, Accepted February 2, 2021*)

Abstract. In this paper, a crack identification using Artificial Neural Network (ANN) is investigated to predict the crack depth in pipeline structure based on modal analysis technique using Finite Element Method (FEM). In various fields, ANN has become one of the most effective instruments using computational intelligence techniques to solve complex problems. This paper uses Particle Swarm Optimization (PSO) to enhance ANN training parameters (bias and weight) by minimizing the difference between actual and desired outputs and then using these parameters to generate the network. The convergence study during the process proves the advantage of using PSO based on two selected parameters. The data are collected from FEM based on different crack depths and locations. The provided technique is validated after collecting the data from experimental modal analysis. To study the effectiveness of ANN-PSO, different hidden layers values are considered to study the sensitivity of the predicted crack depth. The results demonstrate that ANN combined with PSO (ANN-PSO) is accurate and requires a lower computational time in terms of crack identification based on inverse problem.

Keywords: FEM dynamic analysis; experimental modal analysis; crack prediction; ANN; PSO

1. Introduction

Recently, new and creative techniques have been developed for pipeline design due to their importance in transporting energy and water, thus calculation methods have been improved to perform and to design a safe and economical pipeline, which has been often modeled as a beam. The possibility of detecting a crack in L-shaped pipes filled with fluid based on the measurement of transverse natural frequencies, which were provided by (Murigendrappa *et al*. 2005). Damage detection for pipeline structures using optic-based active sensing was presented by Lee and Sohn (2012). Experimental investigations on detecting lateral buckling for subsea pipelines with distributed fiber optic sensors were performed by Feng *et al*. (2015).

Parametric density concept for long-range pipeline health monitoring was presented by Na and Yoon (2007). In fact, the behavior of the pipeline received great attention by researchers due to its wide application in engineering where the crack problems of structures have been extensively studied. Rahman (1997) used a probabilistic approach based on the elastic-plastic FEM in order to predict the pipe crack. (Wang *et al*. 2011) carried out an accurate method based on the genetic algorithm to identify the crack location and size where the efficiency of the method has been proved through experimental results. The remote field eddy current method has been also used to detect the crack in the pipeline (Wu *et al*. 2009). Dilena *et al*. (2011) proposed a method to stabilize the identification of damage parameters of cracked pipe with fluid where a single open crack has been considered. A new technique based on the energy method and the committee network has been also developed by Lee *et al*. (2014) to detect location and size of the crack of a steel cantilever pipe, where 16 damage cases of crack have been chosen. Li *et al*. (2017) carried out the numerical and experimental analyses to identify the damage of the crack in the pipeline by adding virtual masses on the substructure of this later, combined with sensitivity and frequencies. Many different experimental studies have been also done in Refs. (Murigendrappa *et al*. 2004a, b, Pandey and Biswas 1995, Song *et al*. 2006). Moreover, different other methods based on damage identification in order to detect the sensitivity of the damage and to predict the real behavior of the beam have been extensively used. A dynamic and static analysis based on the XIGA has been done by Khatir *et al*. (2020) to improve ANN technique, which has been used to identify the crack length in plates, where different crack scenarios

*Corresponding author, Ph.D.,
E-mail: Samir.khatir@ou.edu.vn
[a] Ph.D., E-mail: meriem.seguini@univ-usto.dz
[b] Professor, E-mail: djilali.boutchicha@gmail.com
[c] Professor, E-mail: djamel.nedjar@univ-usto.dz
[d] Professor, E-mail: magdabdelwahab@duytan.edu.vn; magd.abdelwahab@ugent.be

Copyright © 2021 Techno-Press, Ltd.

ISSN: 1738-1584 (Print), 1738-1991 (Online)

and different boundary conditions have been adopted. Hence the results proved the efficiency of the improved application. Tran-Ngoc *et al.* (2020c) coupled the Orthogonal Diagonalization (OD) with an improved Particle Swarm Optimization (IPSO) for the model updating of a large-scale railway bridge, and the obtained results proved the performance of the developed approach in terms of times and the accuracy.

More recent related researches based on the vibration tests of the model deformation are described in Refs. (Bonnet and Constantinescu 2005, Gillich *et al.* 2016, 2019, Zhou *et al.* 2017, 2018). It is worthwhile to mention that several researchers based on different methods have recently used energy method to identify the crack in a vibrating beam (Yang *et al.* 2001), while other authors used Timoshenko and Euler formulations as in Ref. (Swamidas *et al.* 2004). The forced vibration beam has been also presented in Ref. (Loutridis *et al.* 2005). Galvanetto and Violaris (2007) performed simulation tests on two beams, which provided promising results. The proposed idea is based on the POD theory in order to detect and localize damage in structures. Dougdag *et al.* (2014) carried out a sine-sweep vibration measurement based on a new approach to detect a crack in steel beams. Sinou (2009) established a review of damage detection of a mechanical system based on the linear and nonlinear vibrations measurements. More refined models have been also developed to identify the damage in bridges and beam-like structures using ANN and Cuckoo search algorithm by Tran-Ngoc *et al.* (2019). Several other numerical examples have been also studied by the same authors by using a developed approach in order to identify the damage in different structures (Tran-Ngoc *et al.* 2020a, b). A deep collocation method for the bending analysis of Kirchhoff plate was investigated by Guo *et al.* (2019) and an energy approach to the solution of partial differential equations in computational mechanics via machine learning was investigated by Samaniego *et al.* (2020). Fayyadh *et al.* (2011) proposed a Combined Parameter Index (CPI) to detect the damage severity in beam-like structures in various location. Grey Wolf Optimization algorithm was investigated for damage detection of skeletal structures via expanded mode shapes by Ghannadi *et al.* (2020). Moreover, Structural damage detection based on Modal Assurance Criterion (MAC) flexibility and frequency using moth-flame algorithm was analyzed by Ghannadi and Kourehli (2019).

The main objective of this paper is to propose a more accurate pipe model by using FEM, in order to identify the crack depth in different positions based on ANN-PSO. PSO adapt two parameters (Bias and weight) after collecting the data from a numerical model. The provided technique is tested using an experimental cracked pipe to predict crack angle.

2. PSO-ANN

Artificial Neural Network (ANN) is a statistical methodology developed based on biological nervous systems. The dominant characteristic of ANN means the capacity to learn through experience to improve performance. Therefore, ANN can be applied for a wide range of fields comprising classification, pattern recognition, identification, image processing, and control system. ANN training parameters (bias and weight) can be improved by minimizing the difference between actual and desired outputs and then using these parameters to generate the network using PSO. Each value of training parameters (weight and bias) is considered as a solution that the PSO algorithm is seeking. In this paper, we employed ANN-PSO to predict the crack depth in the pipeline. Basically, a network of ANN has three major components consisting of an input layer, hidden layer, and output layer as shown in Fig. 1.

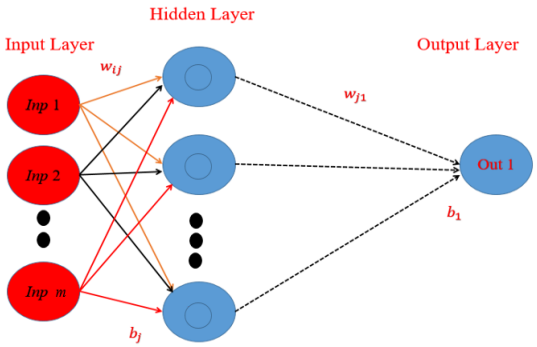

Fig. 1 A typical Artificial Neural Network (ANN) architecture

where, w_{ij} is the weights of neuron connection between an input node and neuron in the hidden layers, b_j is the bias, w_{j1} is the weights of neuron connection between neuron in hidden and output layers. b_1 is the bias associated with the single neuron in output layer. Index i = 1, 2, …, m is the number of collected data and index j = 1, 2, …, n is the number of hidden layer neurons. The total number of parameters (weight and bias) used in the network is $n\times$ (m + 2) + 1. After building the structure of the ANN model, training with known input and the output sets are performed to find the suitable weights and biases using PSO as presented in Ref. (Rukhaiyar *et al.* 2018). The objective is to minimize Root-Mean-Square Error (RMSE) function of the network, which is described by the following formulation

$$\text{RMSE} = \sqrt{\frac{\sum_{l=1}^{n}(O_l - l_l)^2}{nd}} \quad (1)$$

where O_l is the output corresponding to l^{th} data point in the training set by the network, l_l denotes actual output as consider in the target set. nd is the number of data point considered in training data-set.

3. Numerical analysis using FEM (ANSYS)

The pipe has been modeled as 3D FEM using ANSYS V 18.1 as shown in Fig. 2. Various depths of cracks have been created in different locations along the length of the pipe. First, in the middle, second in the left-hand side and finally

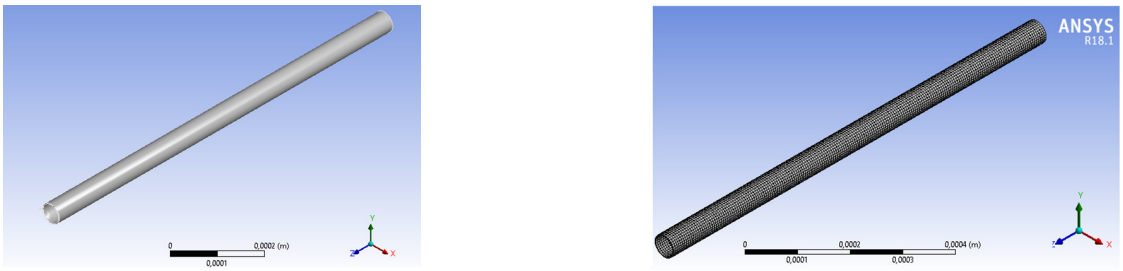

Fig. 2 Finite element model of the pipe

Table 1 Dimensions and material characteristics

Item	Notation	Value
Length (mm)	L_p	1000
Diameter (mm)	D_p	500
Density (kg/m^3)	ρ	7850
Poisson ratio (/)	υ_p	0.3
Young modulus (MPa)	E_p	61950

Table 2 The measured frequencies of the first crack in the middle of the pipe

Mode	FEM	Experimental
1	288.49	289.38
2	774.47	785
3	1460	1463.8

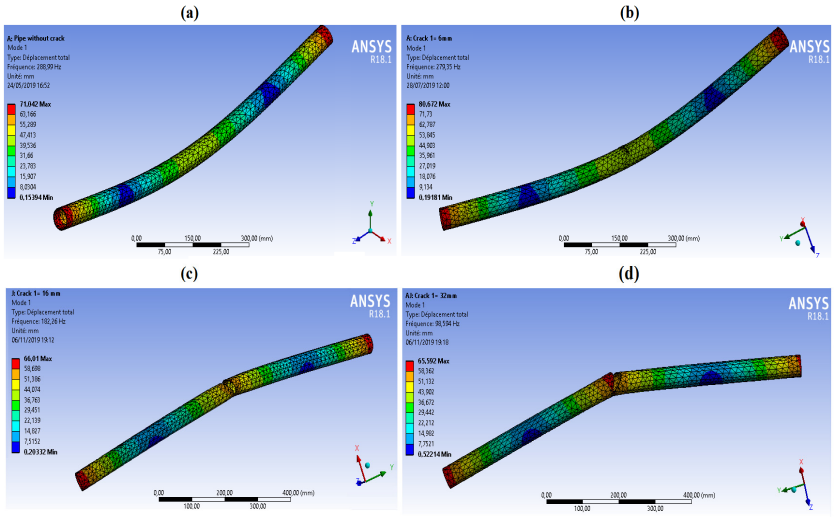

Fig. 3 Natural frequency and the first mode shape: (a) Healthy pipe; (b) Cracked pipe with 6 mm of depth; (c) Cracked pipe with 16 mm of depth; and (d) Cracked pipe with 32 mm of depth (Scenario 1)

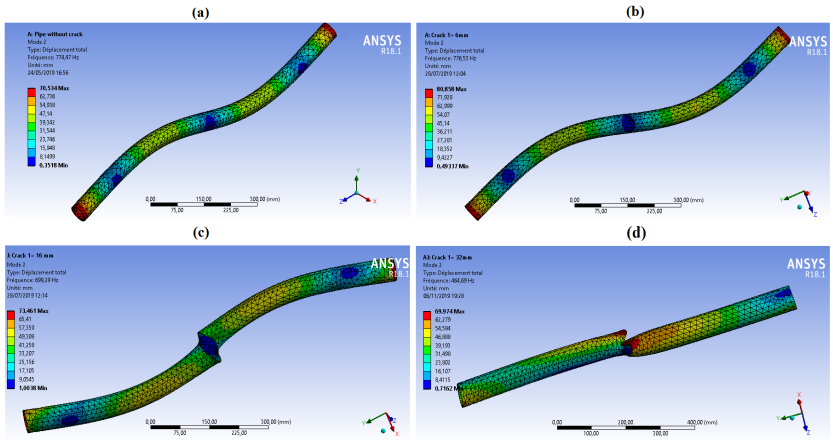

Fig. 4 Natural frequency and the second mode shape: (a) Healthy pipe; (b) Cracked pipe with 6 mm of depth; (c) Cracked pipe with 16 mm of depth; and (d) Cracked pipe with 32 mm of depth (Scenario 1)

in the right side. Each node has 6 degrees of freedom consisting of 3 transitional displacements u, w, v and 3 rotational displacements θ_x, θ_y, θ_z. The tetrahedron mesh type is used in FE model. The mechanical and geometrical properties of the pipe are presented in Table 1. The frequencies for healthy pipe from numerical and experimental analysis is presented in Table 2.

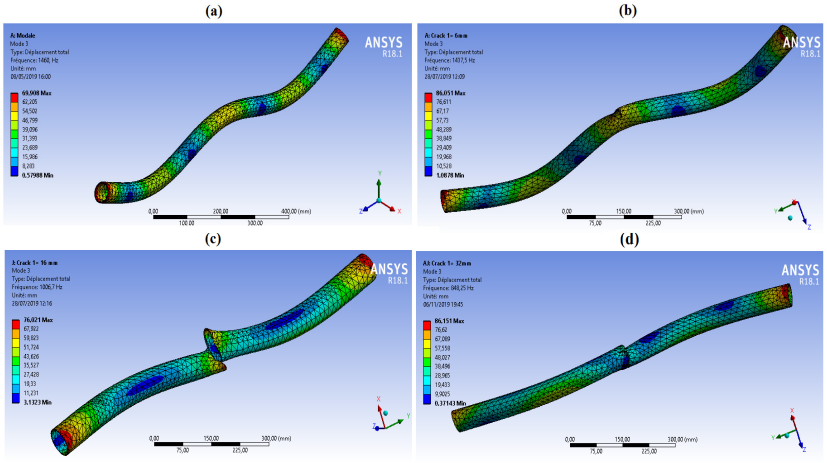

Fig. 5 Natural frequency and the third mode shape: (a) Healthy pipe; (b) Cracked pipe with 6 mm of depth; (c) Cracked pipe with 16 mm of depth; and (d) Cracked pipe with 32 mm of depth (Scenario 1)

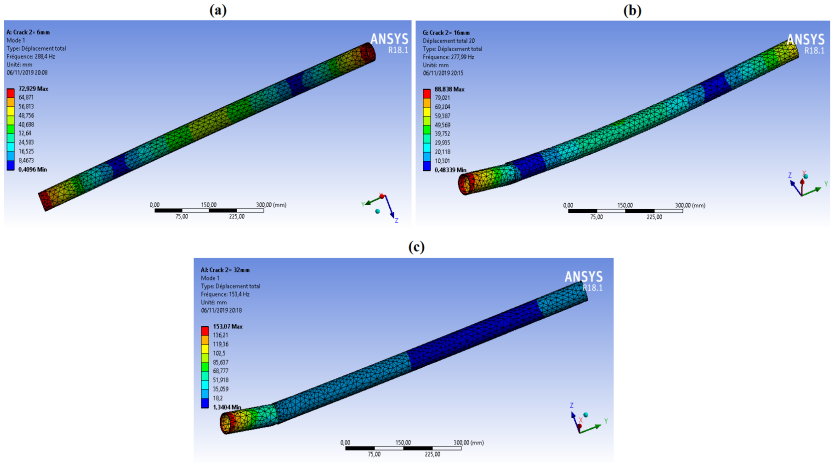

Fig. 6 Natural frequency and the first mode shape: (a) Healthy pipe; (b) Cracked pipe with 6 mm of depth; (c) Cracked pipe with 16 mm of depth; and (d) Cracked pipe with 32 mm of depth (Scenario 2)

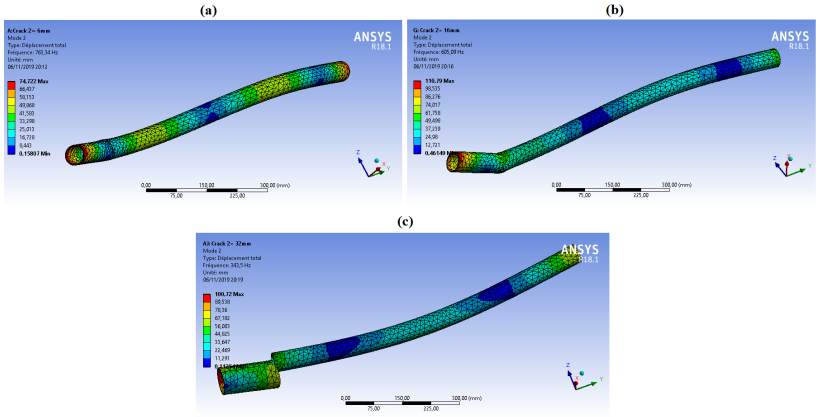

Fig. 7 Natural frequency and the second mode shape: (a) Healthy pipe; (b) Cracked pipe with 6 mm of depth; (c) Cracked pipe with 16 mm of depth; and (d) Cracked pipe with 32 mm of depth (Scenario 2)

3.1 Cracked pipe

Three scenarios are considered to analyze the approach of ANN-PSO for crack depth prediction. In the first scenario, the crack was created in the middle by extending the crack from 2 mm to 32 mm with 0.25 mm step. The frequencies of each crack depth are presented in appendix B. Some mode shapes are presented in Figs. 3-5.

In the second scenario, the crack was created in the left-hand side, which has been extended from 2 mm to 32 mm with 0.25 mm step. The frequencies of each crack depth are presented in appendix B. Some mode shapes are presented

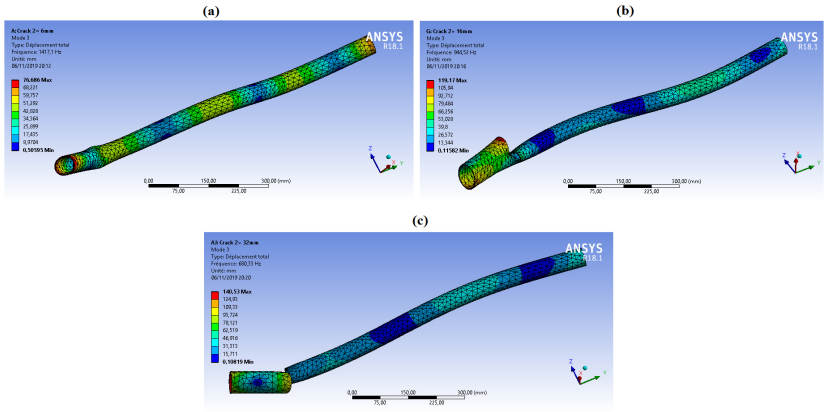

Fig. 8 Natural frequency and the third mode shape: (a) Healthy pipe; (b) Cracked pipe with 6 mm of depth; (c) Cracked pipe with 16 mm of depth; and (d) Cracked pipe with 32 mm of depth (Scenario 2)

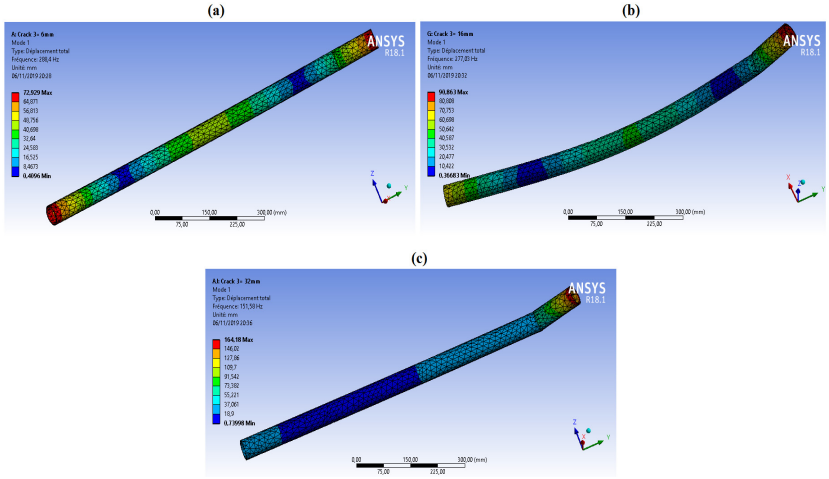

Fig. 9 Natural frequency and the first mode shape: (a) Healthy pipe; (b) Cracked pipe with 6 mm of depth; (c) Cracked pipe with 16 mm of depth; and (d) Cracked pipe with 32 mm of depth (Scenario 3)

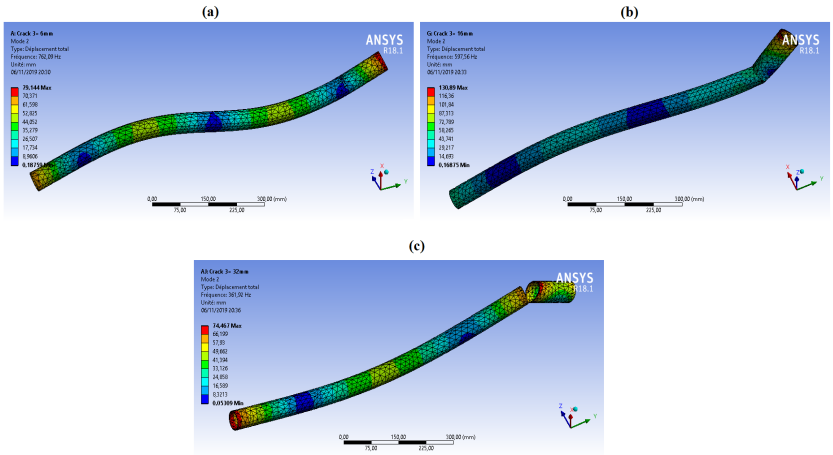

Fig. 10 Natural frequency and the second mode shape: (a) Healthy pipe; (b) Cracked pipe with 6 mm of depth; (c) Cracked pipe with 16 mm of depth; and (d) Cracked pipe with 32 mm of depth (Scenario 3)

in Figs. 6-8.

In the third scenario, the crack was created on the right-hand side, which has been extended from 2 mm to 32 mm with 0.25 mm step. The frequencies for each crack depth are presented in appendix B. The mode shapes of the first three modes with 6 mm, 16 mm and 32 mm are presented in Figs. 9-11.

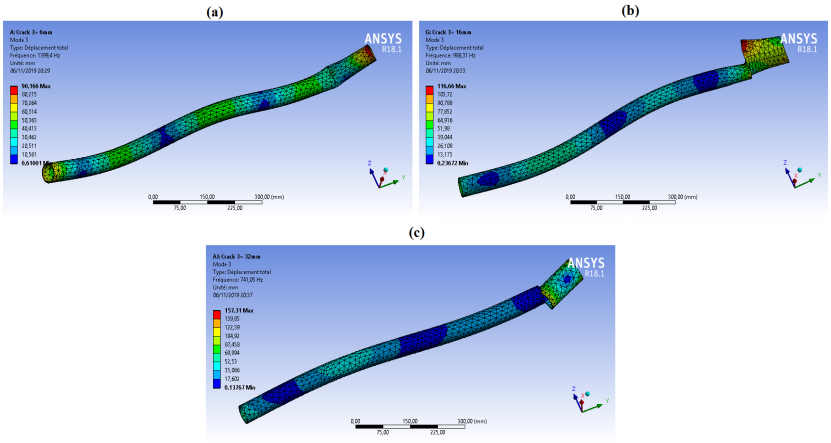

Fig. 11 Natural frequency and the third mode shape: (a) Healthy pipe; (b) Cracked pipe with 6 mm of depth; (c) Cracked pipe with 16 mm of depth; and (d) Cracked pipe with 32 mm of depth. (Scenario 3)

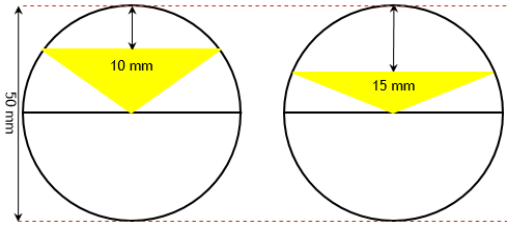

Fig. 12 Crack depth presentation

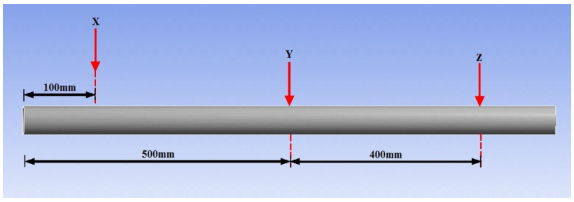

Fig. 13 Pipeline with three zones of extended crack depth (X) zone 1 (Scenario 2), (Y) zone 2 (Scenario 1) and (Z) zone 3 (Scenario 3)

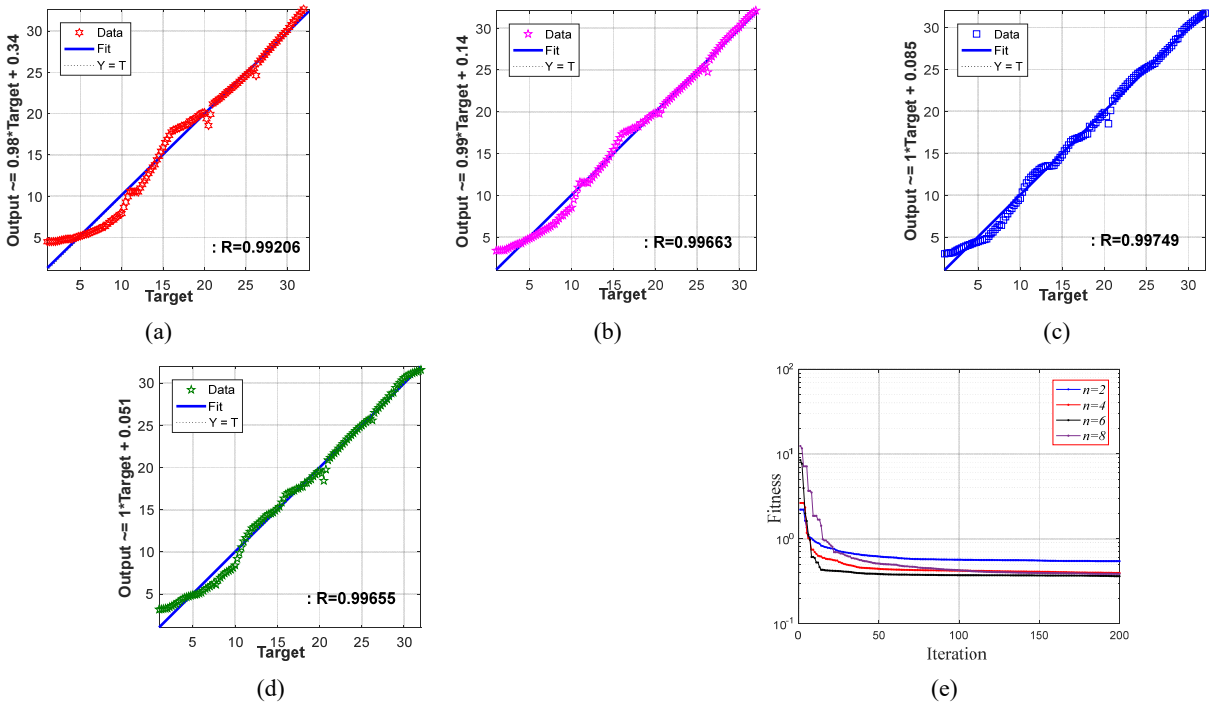

Fig. 14 Regression using different number of Hidden layer size (Zone 2) Middle (a) $n = 2$; (b) $n = 4$; (c) $n = 6$; (d) $n = 8$; and (e) convergence using PSO for each n

3.2 Results and discussion

Based on the analysed results of different scenarios, the datasets are collected to predict the crack depth for each zone as presented in Figs. 12-13. Three scenarios are considered by extending the crack depth as shown in Fig. 13 and Table 3. The sensitivity of n (Number of Hidden layer size) is also investigated using 2, 4, 6, and 8. The number of population and generation is fixed to 200.

Table 3 The considered crack depth

Damage scenario	Crack depth (mm)
1	5
	28.5
2	4
	25
3	6
	30.5

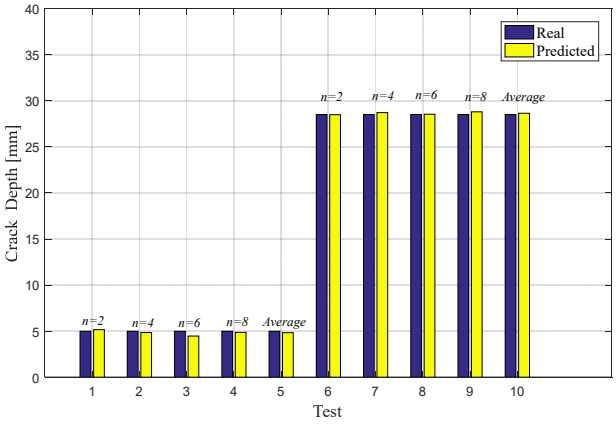

Fig. 15 Real and predicted crack depth by changing the hidden layer size for Scenario 1

3.2.1 Scenario 1

In the first scenario, we predicted two cracks depths as listed in Table 3. The regression of ANN-PSO of each Hidden layer size is presented in Figs. 14(a)-(d) as well as the convergence study of PSO for each Hidden layer size in Fig. 14(e). The results are summarized in Table 4.

The provided results for each test show that the regression is very close to 1 and that the best convergence study is for $n = 6$.

The results showed that ANN improved by PSO can

Table 4 Predicted crack depth for scenario 1

Scenario	Zone	n	Test	Real crack depth	Predicted crack depth
1	2	2	1	5	5.17
		4	2	5	4.86
		6	3	5	4.47
		8	4	5	4.87
		A	5	5	4.84
		2	6	28.5	28.49
		4	7	28.5	28.72
		6	8	28.5	28.55
		8	9	28.5	28.80
		A	10	28.5	28.64

*Notation: A: Average

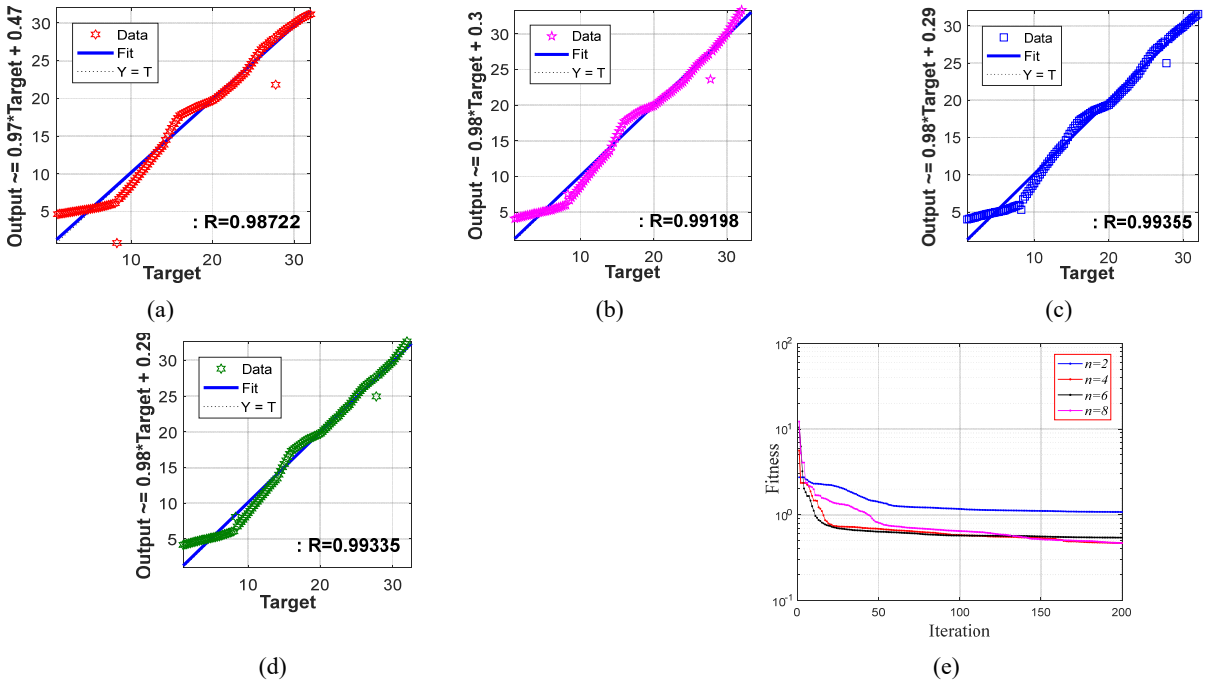

(a) (b) (c) (d) (e)

Fig. 16 Regression using different numbers of Hidden layer size (Zone 1) Left (a) $n = 2$; (b) $n = 4$; (c) $n = 6$; (d) $n = 8$; and (e) convergence using PSO for each n

Table 5 Predicted crack for scenario 2

Scenario	Zone	*n*	Test	Real crack depth	Predicted crack depth
2	1	2	1	4	4.35
		4	2	4	4.32
		6	3	4	4.34
		8	4	4	4.16
		A	5	4	4.29
		2	6	25	24.64
		4	7	25	25.15
		6	8	25	24.80
		8	9	25	25.25
		A	10	25	24.96

*Notation: A: Average

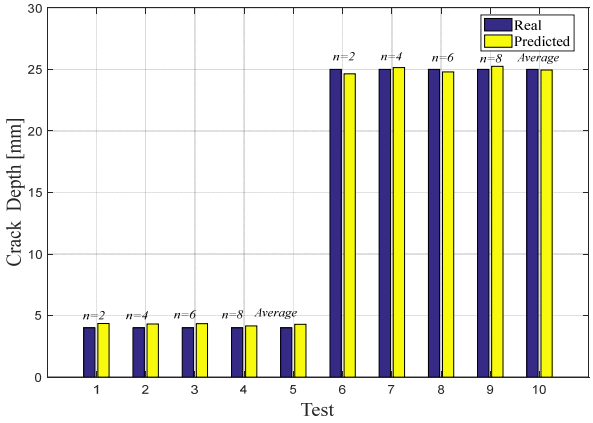

Fig. 17 Real and predicted crack depth by changing the hidden layer size for Scenario 2

predict the crack accurately using different hidden layer size. The results are summarized in Fig. 15.

3.5.2 Scenario 2

In the second scenario, the number of hidden layers is modified from 2 to 8 with step 2 for two predicted cracks depth. The regression of ANN-PSO is presented in Fig. 16. The predicted results are presented in Table 5.

The obtained results for zone 1 are more accurate based on the regression value for *n*. The best convergence is found for *n* = 8 compared with others.

Based on the provided results, ANN-PSO can predict the crack using different hidden layers. The results are summarized in Fig. 17.

Table 6 Predicted crack for scenario 3

Scenario	Zone	*n*	Test	Real crack depth	Predicted crack depth
3	3	2	1	6	5.92
		4	2	6	6.12
		6	3	6	6.21
		8	4	6	5.97
		A	5	6	6.04
		2	6	30.5	30.23
		4	7	30.5	30.59
		6	8	30.5	30.12
		8	9	30.5	30.45
		A	10	30.5	30.34

*Notation: A: Average

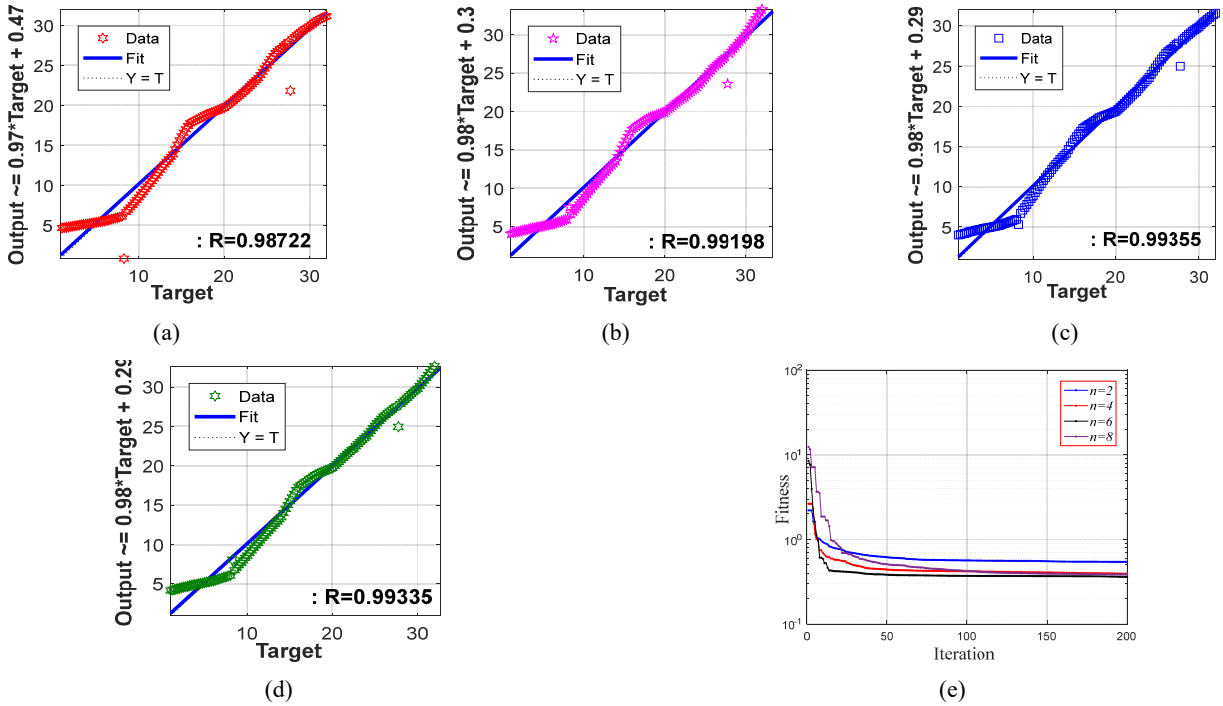

(a) (b) (c) (d) (e)

Fig. 18 Regression using different number of Hidden layer size (Zone 3) Left (a) *n* = 2; (b) *n* = 4; (c) *n* = 6; (d) *n* = 8; and (e) convergence using PSO for each *n*

3.5.3 Scenario 3

In the last scenario, the regressions of ANN-PSO of each Hidden layer size are presented in Fig. 18. The predicted results are provided in Table 6.

It can be seen that PSO provides accurate results for n = 6 based on the convergence study and regression value compared with others.

Based on the found results, we can conclude that ANN-PSO can predict the crack depth 5 mm and 28.5 mm accurately for different hidden layer sizes. The provided results are summarized in Fig. 19.

In summary, based convergence study, PSO can improve the training of ANN during the process using different numbers of hidden layer size.

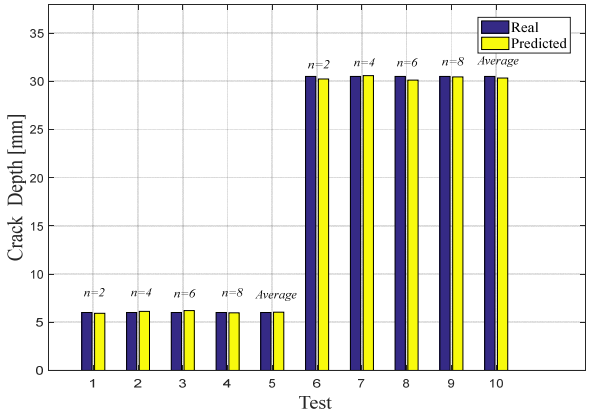

Fig. 19 Real and predicted crack depth by changing the hidden layer size for scenario 3

Fig. 20 Setup modal analysis of cracked pipe

4. Experimental validation

In this study, the experimental modal analysis tests of free-free pipe have been done by using M+P SO Analyzer 4.3, PCB Accelerometers 356A15 and Hammer PCB 086C03 in order to generate the 11 excitations as shown in Fig. 20. The accelerometer is located in the middle of the pipe to determine the frequencies using 16 crack depths (see Fig. 20). The mechanical characteristics are presented in Table 1. Table 7 presents the crack angle of the considered

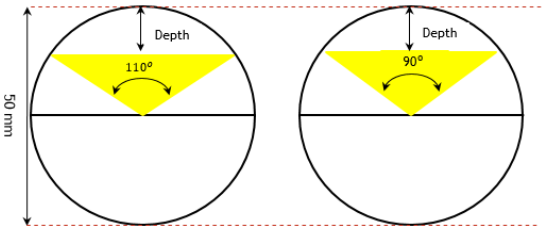

Fig. 21 Crack angle and depth

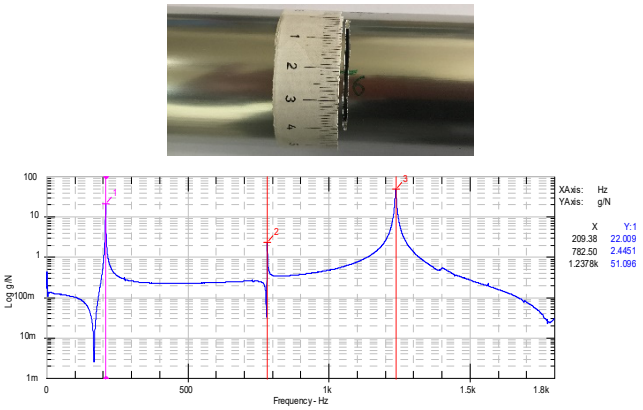

Fig. 22 Crack depth 14 mm with a length of crack l = 40 mm

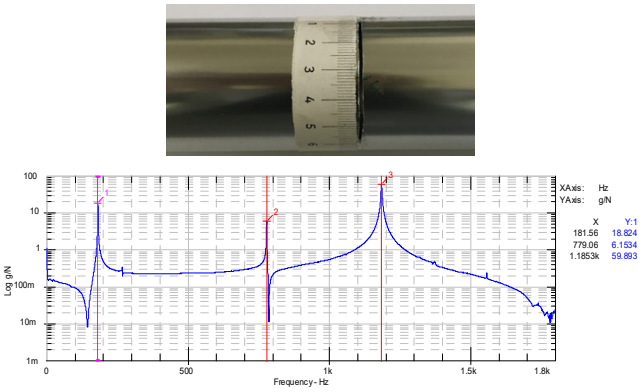

Fig. 22 Crack depth 14 mm with a length of crack l = 40 mm

Table 7 Considered scenarios

Scenario	Crack angle
1	73.74°
2	160.42°

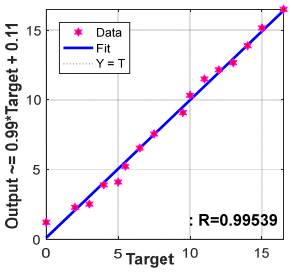

(a)

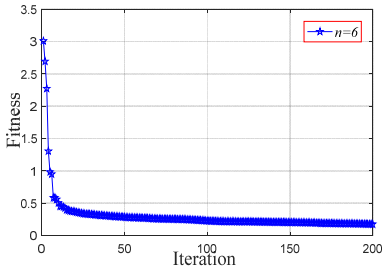

(b)

Fig. 24 Regression ANN-PSO (a) and fitness (b)

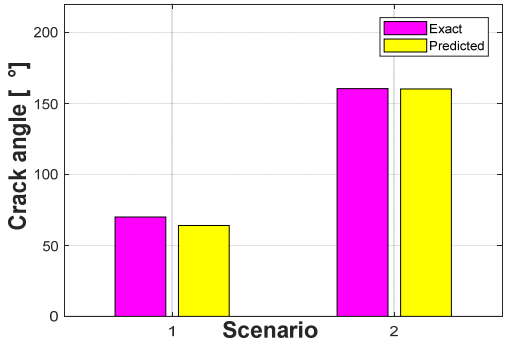

Fig. 25 Predicted crack angle using ANN-PSO

scenarios. Figs. 22 and 23 show Frequency Response Function (FRF) of the cracked pipe with 14 mm and 16 mm depth of crack respectively.

4.1 Results and discussion

In these section two scenarios are considered to predict the angle of the crack based on the frequency measured from the experimental modal analysis as presented in Appendix C. The parameters of ANN-PSO are fixed using 200 populations and iteration, acceleration factor: $c1 = c2 = 1.5$, and a best Hidden layer size of 6. The regression after selecting these parameters is presented in Fig. 24(a) as well the convergence study of PSO in Fig. 24(b). The predicted crack angles are presented in Fig. 25.

PSO provides accurate results for $n = 6$ based on actual and predicted crack angles. Based on the previous results the training can be improved after adapting two parameters bias and weight using PSO.

5. Conclusions

This paper investigates the prediction of crack depth and angle using ANN improved by PSO. FE model of cracked pipe with different scenarios is provided in this paper. The crack depth is extended in each scenario in order to help to collect data for ANN-PSO. The method is based on frequencies, which are used as input data and crack depth as output. To test the accuracy of improved method, experimental modal analysis was performed to collect the data for ANN-PSO by creating a crack in the middle of the pipe and extending the crack angle from 46° to 183.34°. The results show an accurate prediction of the crack angle based on two scenarios of 73.74° and 160.42°. Regarding convergence, PSO can improve the training during the process using different numbers of hidden layer size.

References

Bonnet, M. and Constantinescu, A. (2005), "Inverse problems in elasticity", *Inverse Problems*, **21**, R1. https://doi.org/10.1088/0266-5611/21/2/r01

Dilena, M., Dell'Oste, M.F. and Morassi, A. (2011), "Detecting cracks in pipes filled with fluid from changes in natural frequencies", *J. Mech. Syst.*, **25**, 3186-3197. https://doi.org/10.1016/j.ymssp.2011.04.013

Dougdag, M., Ouali, M., Mellel, N. and Attari, K. (2014), "Détection de fissures dans les poutres d'acier: une nouvelle approche par balayage de mesures de vibrations", *Mech. Reports*, **342**(8), 437-449. https://doi.org/10.1016/j.crme.2014.05.001

Fayyadh, M.M., Razak, H.A. and Ismail, Z. (2011), "Combined modal parameters-based index for damage identification in a beamlike structure: theoretical development and verification", *J. Arch. Civil Mech. Eng.*, **11**, 587-609. https://doi.org/10.1016/s1644-9665(12)60103-4

Feng, X., Wu, W., Li, X., Zhang, X. and Zhou, J. (2015), "Experimental investigations on detecting lateral buckling for subsea pipelines with distributed fiber optic sensors", *Smart Struct. Syst., Int. J.*, **15**(2), 245-258. https://doi.org/10.12989/sss.2015.15.2.245

Ghannadi, P. and Kourehli, S.S. (2019), "Structural damage detection based on MAC flexibility and frequency using moth-flame algorithm", *Struct. Eng. Mech., Int. J.*, **70**(6), 649-659. https://doi.org/10.12989/sem.2019.70.6.649

Ghannadi, P., Kourehli, S.S., Noori, M. and Altabey, W.A. (2020), "Efficiency of grey wolf optimization algorithm for damage detection of skeletal structures via expanded mode shapes", *Adv. Struct. Eng.*, 1369433220921000. https://doi.org/10.1177/1369433220921000

Galvanetto, U. and Violaris, G. (2007), "Numerical investigation of a new damage detection method based on proper orthogonal decomposition", *J. Mech. Syst. Signal Process.*, **21**, 1346-1361. https://doi.org/10.1016/j.ymssp.2005.12.007

Gillich, G.R., Praisach, Z.I., Abdel Wahab, M., Gillich, N., Mituletu, I.C. and Nitescu, C. (2016), "Free vibration of a perfectly clamped-free beam with stepwise eccentric distributed masses", *J. Shock Vib.*, 2016. https://doi.org/10.1155/2016/2086274

Gillich, G.R., Furdui, H., Wahab, M.A. and Korka, Z.I. (2019), "A

robust damage detection method based on multi-modal analysis in variable temperature conditions", *Mech. Syst. Signal Process*., **115**, 361-379. https://doi.org/10.1016/j.ymssp.2018.05.037

Guo, H., Zhuang, X. and Rabczuk, T. (2019), "A deep collocation method for the bending analysis of Kirchhoff plate", *Comput. Mater. Continua*, **59**(2), 433-456. https://doi:10.32604/cmc.2019.06660

Khatir, S., Boutchicha, D., Le Thanh, C., Tran-Ngoc, H., Nguyen, T.N. and Abdel-Wahab, M. (2020), "Improved ANN technique combined with Jaya algorithm for crack identification in plates using XIGA and experimental analysis", *Theor. Appl. Fract. Mech*., **107**, 102554. https://doi.org/10.1016/j.tafmec.2020.102554

Lee, H. and Sohn, H. (2012), "Damage detection for pipeline structures using optic-based active sensing", *Smart Struct. Syst*., *Int. J*., **9**(5), 461-472. https://doi.org/10.12989/sss.2012.9.5.461

Lee, J.W., Kim, S.R. and Huh, Y.C. (2014), "Pipe crack identification based on the energy method and committee of neural networks", *Int. J. Steel Struct.res*, **14**, 345-354. https://doi.org/10.1007/s13296-014-2014-0

Li, D., Lu, D. and Hou, J. (2017), "Pipeline damage identification based on additional virtual masses", *Appl. Sci*., **7**, 1040. https://doi.org/10.3390/app7101040

Loutridis, S., Douka, E. and Hadjileontiadis, L.J. (2005), "Forced vibration behaviour and crack detection of cracked beams using instantaneous frequency", *J. Ndt & E International*, **38**, 411-419. https://doi.org/10.1016/j.ndteint.2004.11.004

Murigendrappa, S.M., Maiti, S.K. and Srirangarajan, H.R. (2004a), "Experimental and theoretical study on crack detection in pipes filled with fluid", *J. Sound Vib*., **270**, 1013-1032. https://doi.org/10.1016/s0022-460x(03)00198-6

Murigendrappa, S.M., Maiti, S.K. and Srirangarajan, H.R. (2004b), "Frequency-based experimental and theoretical identification of multiple cracks in straight pipes filled with fluid", *J. Ndt & E International*, **37**, 431-438. https://doi.org/10.1016/j.ndteint.2003.11.009

Murigendrappa, S.M., Maiti, S.K. and Srirangarajan, H.R. (2005), "Detection of crack in L-shaped pipes filled with fluid based on transverse natural frequencies", *Struct. Eng. Mech*., *Int. J*., **21**(6), 635-658. https://doi.org/10.12989/sem.2005.21.6.635

Na, W.B. and Yoon, H.S. (2007), "Parametric density concept for long-range pipeline health monitoring", *Smart Struct. Syst*., *Int. J*., **3**(3), 357-372. https://doi.org/10.12989/sss.2007.3.3.357

Pandey, A.K. and Biswas, M. (1995), "Experimental verification of flexibility difference method for locating damage in structures", *J. Sound Vib*., **184**, 311-328. https://doi.org/10.1006/jsvi.1995.0319

Rahman, S. (1997), "Probabilistic fracture analysis of cracked pipes with circumferential flaws", *Int. J. Press. Vessels Piping*, **70**, 223-236. https://doi.org/10.1016/s0308-0161(96)00034-8

Rukhaiyar S, Alam M and Samadhiya N. (2018), "A PSO-ANN hybrid model for predicting factor of safety of slope", *Int. J. Geotech. Eng*., **12**, 556-566. https://doi.org/10.1080/19386362.2017.1305652

Samaniego, E., Anitescu, C., Goswami, S., Nguyen-Thanh, V.M., Guo, H., Hamdia, K., Zhuang, X. and Rabczuk, T. (2020), "An energy approach to the solution of partial differential equations in computational mechanics via machine learning: Concepts, implementation and applications", *Comput. Methods Appl. Mech. Eng*., **362**, 112790. https://doi.org/10.1016/j.cma.2019.112790

Sinou, J.J. (2009), "A review of damage detection and health monitoring of mechanical systems from changes in the measurement of linear and non-linear vibrations", *Mech. Vib.: Measure. Effects Control*, 643-702.

Song, X., Huang, S. and Zhao, W. (2006), "Nondestructive testing technique for cracks in long-distance natural gas pipelines", *J. Nat. Gas Ind*., **26**(7), 103-106. https://doi.org/10.1007/bf02830170

Swamidas, A.S.J., Yang, X. and Seshadri, R. (2004), "Identification of cracking in beam structures using Timoshenko and Euler formulations", *J. Eng. Mech*., **130**, 1297-1308. https://doi.org/10.1061/(asce)07339399(2004)130:11(1297)

Tran-Ngoc, H., Khatir, S., De Roeck, G., Bui-Tien, T. and Wahab, M.A. (2019), "An efficient artificial neural network for damage detection in bridges and beam-like structures by improving training parameters using cuckoo search algorithm", *Eng. Struct*., **199**, 109637. https://doi.org/10.1016/j.engstruct.2019.109637

Tran-Ngoc, H., Khatir, S., Ho-Khac, H., De Roeck, G., Bui-Tien, T. and Wahab, M.A. (2020a), "Efficient Artificial neural networks based on a hybrid metaheuristic optimization algorithm for damage detection in laminated composite structures", *Compos. Struct. J*., 113339. https://doi.org/10.1016/j.compstruct.2020.113339

Tran-Ngoc, H., Khatir, S., Le-Xuan, T., De Roeck, G., Bui-Tien, T. and Wahab, M.A. (2020b), "A novel machine-learning based on the global search techniques using vectorized data for damage detection in structures", *Int. J. Eng. Sci*., **157**, 103376. https://doi.org/10.1016/j.ijengsci.2020.103376

Tran-Ngoc, H., He, L., Reynders, E., Khatir, S., Le-Xuan, T., De Roeck, G., Bui-Tien, T. and Wahab, M.A. (2020c), "An efficient approach to model updating for a multispan railway bridge using orthogonal diagonalization combined with improved particle swarm optimization", *J. Sound Vib*., **476**, 115315. https://doi.org/10.1016/j.jsv.2020.115315

Wang, Y.M., Chen, X.F. and He, Z.J. (2011), "Dubechies wavelet finite element method and genetic algorithm for detection of pipe crack", *J. Nondestruct. Test. Eval*., **26**, 87-99.

Wu, D.H., Huang, S.L., Zhao, W. and Liu, H.Q. (2009), "Research on 3-D simulation of remote field eddy current detection for pipeline cracks", *J. Syst. Simul*., **21**, 6626-6629. https://doi.org/10.4028/www.scientific.net/amr.760-762.1154

Yang, X.F., Swamidas, A.S.J. and Seshadri, R. (2001), "Crack identification in vibrating beams using the energy method", *J. Sound Vib*., **244**, 339-357. https://doi.org/10.1006/jsvi.2000.3498

Zhou, Y.L., Maia, N.M., Sampaio, R.P. and Wahab, M.A. (2017), "Structural damage detection using transmissibility together with hierarchical clustering analysis and similarity measure", *Struct. Health Monitor*., **16**, 711-731. https://doi.org/10.1177/1475921716680849

Zhou, Y.L., Maia, N.M. and Abdel Wahab, M. (2018), "Damage detection using transmissibility compressed by principal component analysis enhanced with distance measure", *J. Vib. Control*, **24**, 2001-2019. https://doi.org/10.1177/1077546316674544

HJ

Appendix

A - The first Three mode shapes of predicted crack depth for different sides

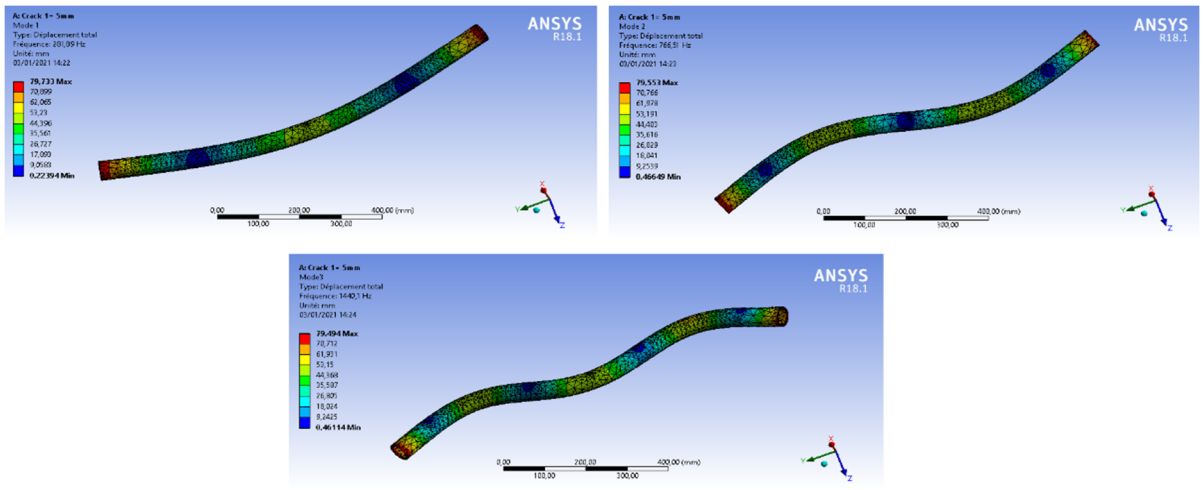

5 mm (Middle)

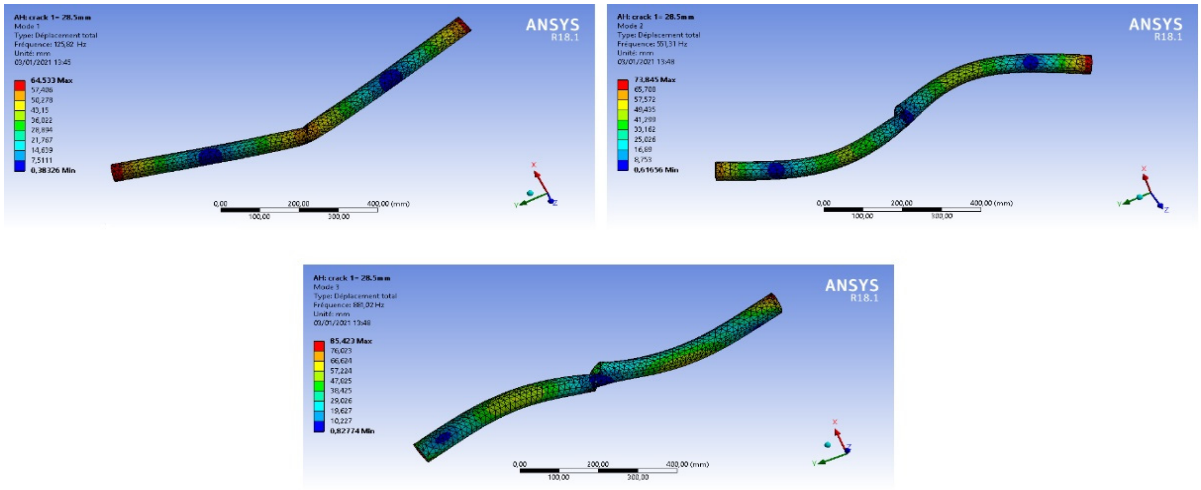

28.5 mm (Middle)

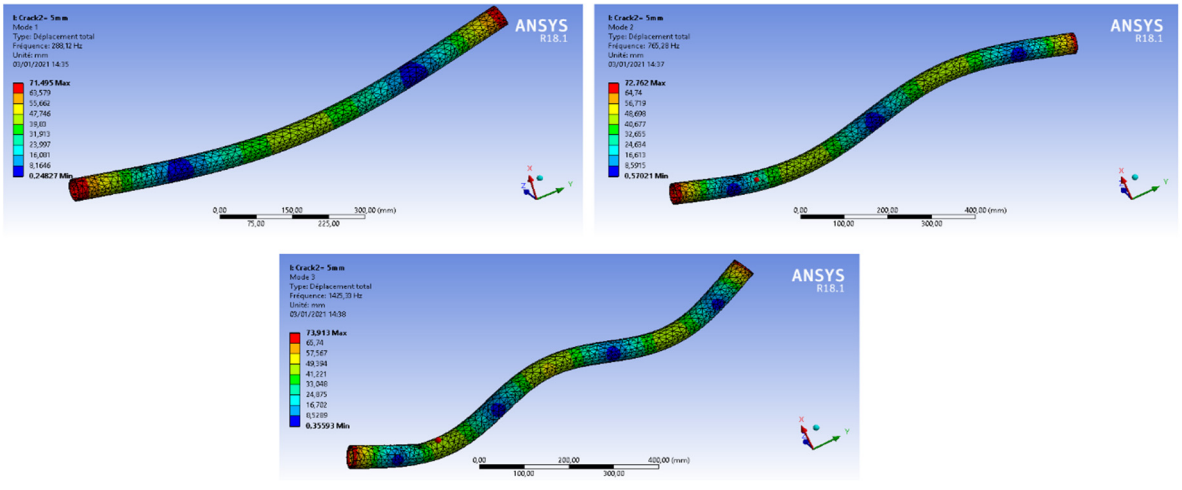

5 mm (Left)

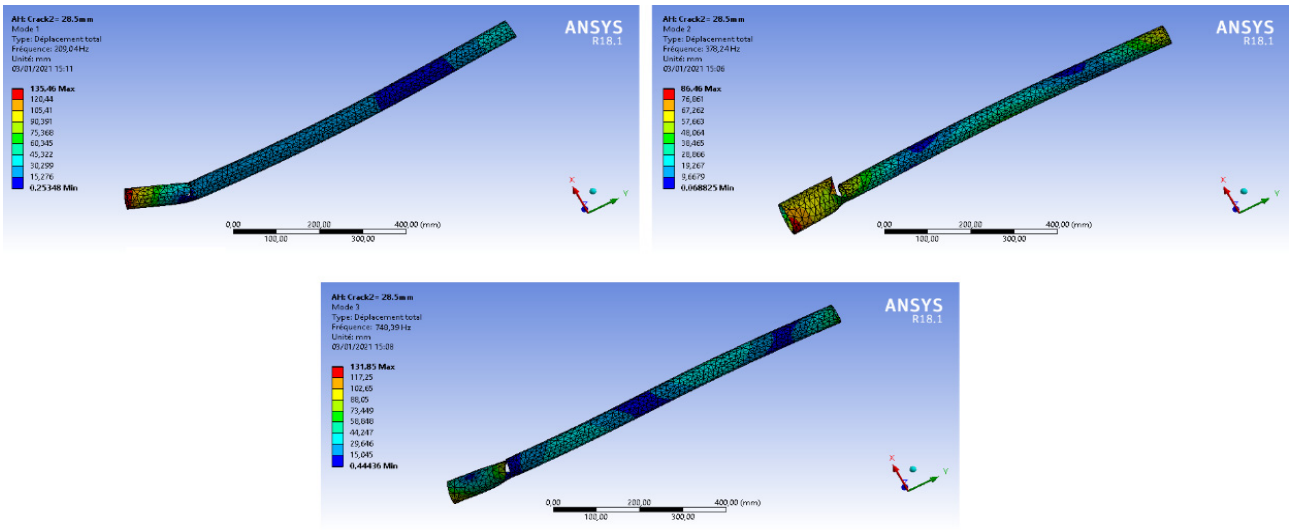

28.5 mm (Left)

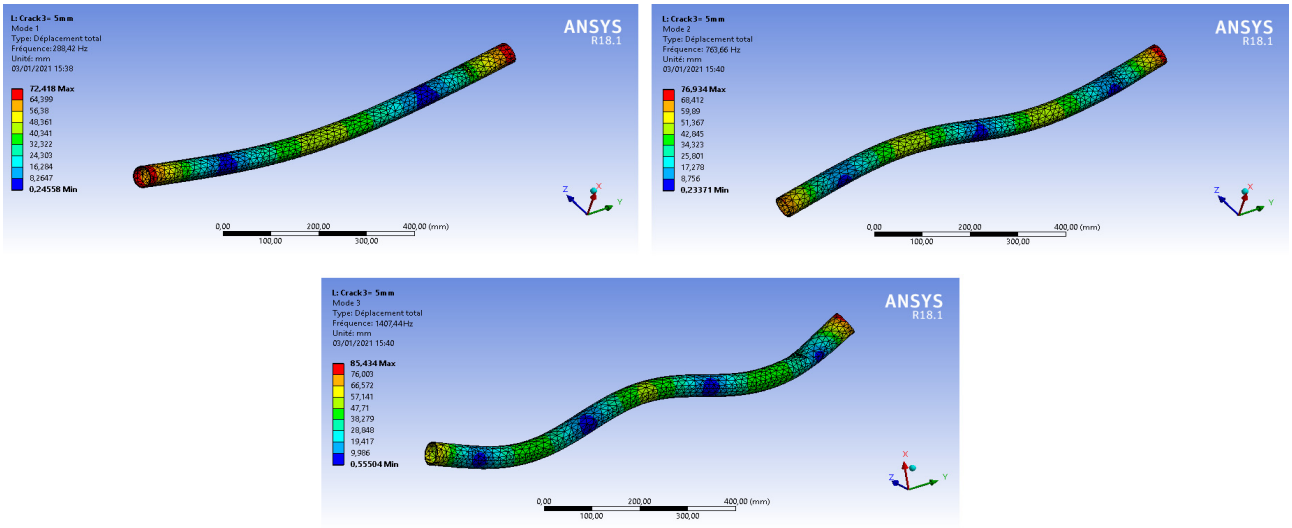

5 mm (Right)

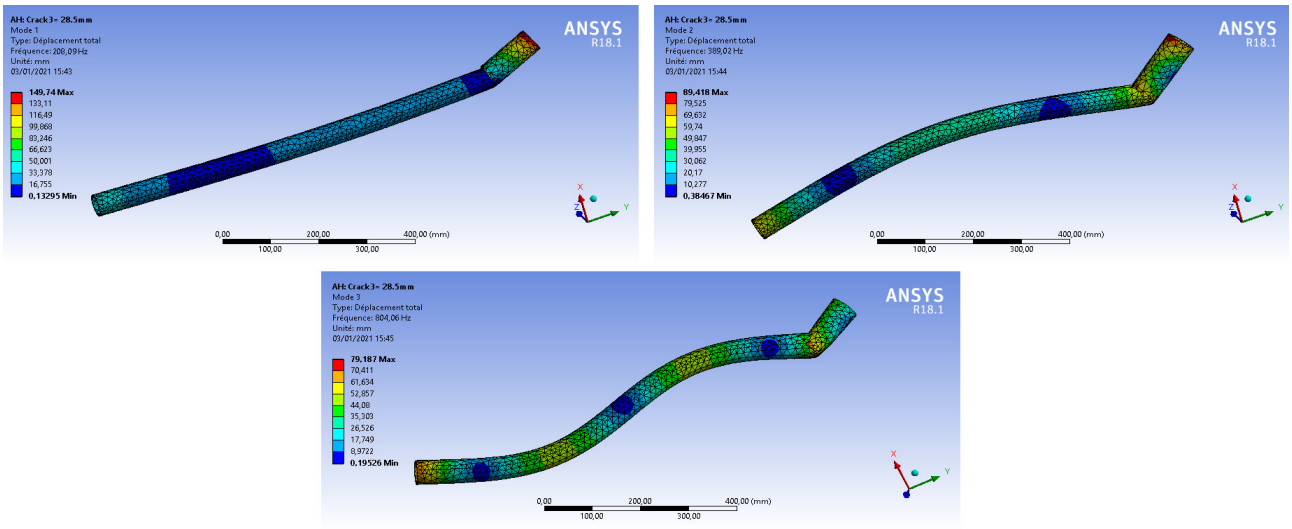

28.5 mm (Right)

B - Frequencies of different cracks depth for each location

Crack Depth	Middle crack			Left crack			Right crack		
	Mode 1	Mode 2	Mode 3	Mode 1	Mode 2	Mode 3	Mode 1	Mode 2	Mode 3
1	288.99	774.47	1460	288.99	774.47	1460	288.99	774.47	1460
1.25	288.89	774.37	1459.17	288.912	773.781	1456.87	288.90	773.69	1456.88
1.5	288.75	774.33	1458.43	288.81	773.20	1455.93	288.86	773.02	1453.87
1.75	288.65	774.27	1457.689	288.73	772.48	1453.84	288.79	772.24	1450.48
2	288.59	774.25	1457	288.69	771.99	1451.9	288.76	771.55	1447.2
2.25	287.912	774.27	1454.97	288.47	771.02	1449.1	288.71	770.968	1443.18
2.5	287.335	774.31	1453.01	288.39	770.42	1447.10	288.65	769.90	1439.24
2.75	286.623	774.33	1451.301	288.371	769.88	1444.79	288.628	769.08	1435.28
3	286.12	774.37	1449.5	288.36	769.49	1442.78	288.61	768.401	1431.41
3.25	285.536	774.91	1447.643	288.279	768.66	1440.10	288.558	767.58	1427.399
3.5	285.15	775.43	1446.19	288.232	768.103	1438.019	288.52	766.80	1423.50
3.75	284.72	775.895	1444.398	288.165	767.59	1435.79	288.505	766.01	1419.52
4	284.69	776.5	1443	288.13	767.29	1433.9	288.49	765.32	1415.7
4.25	283.779	776.491	1442.1	288.1291	766.66	1431.29	288.46	764.81	1413.54
4.5	283.102	776.480	1441.38	288.1282	766.192	1429.51	288.45	764.38	1411.52
4.75	282.399	776.465	1440.77	288.127	765.672	1427.08	288.432	764.12	1409.29
5	281.89	776.513	1440.1	288.126	765.285	1425.33	288.423	763.66	1407.44
5.25	281.225	776.232	1439.17	288.1243	764.691	1423.13	288.417	763.27	1405.345
5.5	280.48	776	1438.5	288.1229	764.21	1421.11	288.412	762.859	1403.383
5.75	279.913	776.255	1437.95	288.12145	763.66	1418.89	288.403	762.42	1401.312
6	279.35	776.53	1437.5	288.12	763.34	1417.1	288.4	762.09	1399.4
6.25	278.199	775.651	1431.6	288.01	762.4	1413.39	288.312	761.60	1397.32
6.5	277.179	775.02	1426.03	287.88	761.63	1410.1	288.29	761.17	1395.37
6.75	276.19	774.225	1422.10	287.84	760.78	1407.01	288.262	760.612	1393.29
7	275.201	773.231	1416.13	287.82	760.08	1404.36	288.256	760.32	1391.51
7.25	274.214	772.401	1411.38	287.65	759.09	1401.11	288.231	759.74	1389.541
7.5	273.123	771.581	1404.91	287.64	758.40	1397.98	288.214	759.45	1387.57
7.75	272.195	771.15	1408.98	287.612	757.53	1394.76	288.186	759.04	1385.61
8	271.12	770.47	1394.5	287.59	756.88	1391.7	288.17	758.69	1383.8
8.25	268.88	769.02	1387.65	287.28	753.599	2761.06	287.86	755.312	1369.587
8.5	267.09	767.98	1380.99	287.01	750.351	1369.701	287.71	752.06	1355.498
8.75	265.1	767	1374.1	286.66	747.029	1358.799	287.51	748.76	1341.391
9	264.47	765.99	1367.8	286.53	744.109	1348.09	287.357	745.6	1327.37
9.25	262.37	764.31	1361.10	286.275	740.83	1337.07	287.173	742.48	1313.21
9.5	261.01	763.1	1355.02	286.012	737.68	1326.29	286.99	739.42	1299.214
9.75	259.11	762.05	1348.95	285.78	734.42	1315.37	286.81	736.293	1285.124
10	258.04	761.91	1343.1	285.7	731.39	1304.6	286.68	733.31	1271.1
10.25	252.15	761.046	1328.89	285.31	727.392	1294.359	286.291	725.123	1250.489
10.5	247.131	760.162	1314.98	284.98	723.78	1284.398	285.93	717.12	1230
10.75	242.05	759.503	1300.95	284.651	719.98	1274.204	285.59	709.03	1209.47
11	237.01	759.11	1287.125	284.41	716.36	1264.29	285.31	701.1	1189.02
11.25	236.40	758.52	1272.975	284.01	712.498	1254.139	284.87	693.36	1168.34
11.5	235.195	758.13	1259.10	283.71	708.77	1244.148	284.57	685.754	1147.92
11.75	234.03	757.06	1245.1	283.39	705.02	1234.035	284.32	678.13	1127.32
12	233.47	757	1231.5	283.19	701.38	1224.1	284.01	670.69	1107

Crack Depth	Middle crack			Left crack			Right crack		
	Mode 1	Mode 2	Mode 3	Mode 1	Mode 2	Mode 3	Mode 1	Mode 2	Mode 3
12.25	**230.01**	**754.12**	**1219.14**	**282.79**	**696.803**	**1215.41**	**283.82**	**669.65**	**1104.21**
12.5	226.9	752.01	1206.995	282.491	692.44	1206.879	283.81	668.79	1101.71
12.75	223.57	750.22	1194.97	282.149	687.96	1198.219	283.79	667.85	1099.05
13	220.85	748.34	1183.10	281.88	683.63	1189.893	283.78	667.03	1096.66
13.25	217.01	746.10	1170.79	281.41	679.04	1181.26	283.75	666.02	1094
13.5	214.27	744.58	1159.09	281.179	674.685	1172.76	283.70	665.28	1091.45
13.75	211.01	742.745	1147.03	280.88	670.27	1164.11	283.67	664.42	1088.89
14	208.83	740.92	1136.2	280.63	665.96	1155.8	283.64	663.62	1086.4
14.25	205.013	735.063	1119.176	280.18	658.22	1129.27	282.69	655.27	1073.99
14.5	202.021	730.112	1103.14	279.79	650.60	1102.89	281.89	647.01	1061.80
14.75	198.099	724.75	1086.91	279.37	643.01	1076.40	281.02	638.70	1049.32
15	195.40	720.01	1071.19	279.07	635.48	1050.11	280.287	630.57	1037.32
15.25	191.887	714.42	1064.346	278.60	627.78	1023.67	279.38	345.71	1025.01
15.5	188.495	709.12	1038.879	278.279	620.19	997.29	278.58	614.01	1012.79
15.75	185.178	704.047	1022.45	277.89	612.58	970.869	277.754	605.67	1000.499
16	182.26	699.29	1006.7	277.58	605.09	944.52	277.03	597.56	988.31
16.25	181.03	697.11	1004.10	276.499	600.90	940.390	276.36	589.17	979.07
16.5	180.695	696.15	1001.987	275.50	596.87	936.41	275.78	580.88	970.12
16.75	179.89	695.027	999.568	274.47	592.72	932.388	275.194	572.56	961.01
17	179.49	694.423	997.489	273.53	588.73	928.48	274.59	564.36	952.07
17.25	178.132	692.959	994.40	272.50	584.57	924.35	273.895	555.896	942.975
17.5	178.038	691.853	992.125	271.49	580.50	920.41	273.31	547.69	933.92
17.75	177.09	690.37	990.037	270.48	576.39	916.40	272.71	539.389	924.87
18	176.88	689.7	988.49	269.56	572.45	912.51	272.19	531.21	915.88
18.25	175.643	681.543	985.021	269.3	569.14	908.367	271.576	527.70	914.65
18.5	175.01	683.052	982.13	269.24	566.01	904.30	271.04	524.36	913.7
18.75	174.032	679.01	979.162	269.09	562.78	900.198	270.55	520.91	912.43
19	173.49	677.07	977.5	268.987	559.69	896.19	270.17	517.597	911.88
19.25	172.054	673.19	972.05	268.79	556.39	892.01	269.58	514.27	910.77
19.5	171.28	670.356	967.394	268.64	553.27	888.01	269.08	511.012	909.84
19.75	170.39	667.02	962.08	268.49	550.01	883.91	268.56	507.69	908.90
20	170.24	664.64	957.51	268.43	546.95	879.91	268.13	504.52	908.05
20.25	169.325	661.037	881.09	267.01	541.58	875.797	267.56	502.79	907.55
20.5	168.91	657.99	805.52	265.65	536.294	871.78	267.21	501.24	907
20.75	167.10	654.643	879.499	264.27	530.97	867.69	266.56	499.88	906.56
21	165.80	651.78	954.15	262.97	525.76	863.78	266.45	498.18	906.23
21.25	164.634	648.599	948.79	261.34	520.31	859.68	266.05	496.1	905.62
21.5	163.715	645.419	943.49	260.13	515.07	855.70	265.98	495.02	905.36
21.75	162.491	642.127	938.189	258.798	509.78	851.68	265.81	493.48	904.91
22	161.65	639.15	932.9	257.6	504.64	847.8	265.72	492.05	904.63
22.25	160.14	636.071	930.492	256.70	499.79	842.73	263.532	485.70	897.20
22.5	159.243	633.17	928.348	255.99	495.07	837.80	261.49	479.513	890.02
22.75	158.054	630.09	926.01	254.17	490.27	832.80	259.34	473.289	882.754
23	157.284	627.295	923.98	252.46	485.59	827.94	257.379	467.174	875.73
23.25	156.023	624.134	921.47	251.123	480.73	822.91	255.13	462.61	867.99
23.5	155.032	621.381	919.479	249.89	476.03	817.99	253.223	454.656	861.234

Crack Depth	Middle crack			Left crack			Right crack		
	Mode 1	Mode 2	Mode 3	Mode 1	Mode 2	Mode 3	Mode 1	Mode 2	Mode 3
23.75	153.912	618.27	917.112	248.65	471.27	813.01	251.38	447.99	854
24	152.98	615.62	915.18	247.51	466.61	808.16	249.15	442.34	846.94
24.25	151.47	613.412	913.69	245.405	459.021	803.778	246.03	437.86	843.29
24.5	150.12	611.399	912.512	243.41	451.70	799.479	244	433.97	840.08
24.75	148.754	609.24	911.193	241.31	444.278	795.128	242	428	837.02
25	147.58	607.41	910.12	239.39	436.949	790.949	239.02	425.67	834.696
25.25	146.167	605.279	908.78	237.263	429.418	786.296	237.04	422	831.02
25.5	144.88	603.31	907.59	235.29	422.07	782.327	234	417.08	828.29
25.75	143.436	601.021	906.139	233.275	414.596	778.021	232	414.02	825.03
26	142.25	599.32	905.17	231.33	407.32	773.82	229.16	409.09	822.48
26.25	149.378	594.74	902.52	229.241	404.187	771.276	227.65	406.78	821.4
26.5	138.65	590.46	900.18	227.213	401.09	768.86	225.06	404.87	819.04
26.75	136.799	586.01	897.596	225.185	397.959	776.356	223.03	402.99	817.24
27	135.32	581.84	895.35	223.267	394.97	764.02	221.66	401.01	815.99
27.25	133.49	577.381	892.774	221.11	391.759	761.499	219.59	398.73	814.64
27.5	131.765	572.99	890.38	219.148	388.756	759.17	217.93	396.96	813.88
27.75	130.021	568.67	887.945	217.216	579.998	756.752	216.55	395.17	812.76
28	128.47	564.44	885.63	215.36	382.7	754.46	214.38	393.18	811.17
28.25	127.023	557.76	883.271	212.123	380.345	751.377	211.5	391.09	807.29
28.5	125.82	551.312	881.021	209.045	378.246	748.398	208.09	389.023	804.063
28.75	124.354	548.76	878.71	205.914	376.012	745.379	204.88	386.96	801
29	123.294	538.312	876.599	202.896	373.901	742.476	201.98	385.01	797.98
29.25	121.89	531.64	874.24	199.697	371.629	739.39	198.66	383	795.05
29.5	120.69	525.19	872.09	196.599	369.486	736.488	195.54	381.04	791.29
29.75	119.32	518.43	869.71	193.495	367.298	733.471	192.67	379	788
30	118.19	512.27	867.69	190.49	365.23	730.55	189.7	377.27	785.04
30.25	115.57	506.015	864.994	185.76	362.41	724.19	184.19	374.98	779.09
30.5	113.193	500.123	862.69	181.13	359.72	717.95	180.24	373	774.02
30.75	110.64	494.17	860.17	176.46	356.98	711.62	175	370.77	768.89
31	108.32	488.44	857.92	171.91	354.33	705.41	170.32	369.40	763.99
31.25	105.75	482.291	855.092	167.14	351.51	698.01	165.22	367.03	757.92
31.5	103.39	476.51	852.94	162.59	348.85	692.82	160.55	365.01	752.13
31.75	100.798	470.47	850.39	157.891	346.09	686.491	155.89	363.12	747.06
31	108.32	488.44	857.92	171.91	354.33	705.41	170.32	369.40	763.99
31.25	105.75	482.291	855.092	167.14	351.51	698.01	165.22	367.03	757.92
31.5	103.39	476.51	852.94	162.59	348.85	692.82	160.55	365.01	752.13
31.75	100.798	470.47	850.39	157.891	346.09	686.491	155.89	363.12	747.06
32	98.594	464.69	848.25	153.4	343.5	680.33	151.58	361.92	741.05

C - Experimental measured frequencies of 16 different cracks in depth

Crack and uncracked tests	Crack angle [°]	Crack depth	Mode 1	Mode 2	Mode 3
1	0	0	289.38	785	1463.8
2	46	2	286.59	785	1454.7
3	56.72	3	285.94	785	1454.1
4	65.72	4	283.75	785.31	1447.2
5	73.74	5	281.88	785	1436.3
6	77.92	5.5	278.75	785	1426.3
7	84.8	6.5	275	785	1403.4
8	91.68	7.5	271.56	785	1394.7
9	10.314	9.5	264.06	784.69	1373.8
10	114.6	10	256.56	784.38	1357.8
11	128.34	11	245	784.06	1321.3
12	137.5	12	234.06	783.75	1292.5
13	148.96	13	222.81	783.44	1265.3
14	160.42	14	209.38	782.50	1237.8
15	171.88	15	196.88	781.25	1212.8
16	183.34	16.5	181.56	779.06	1185.3